Infrared spectrum of the $I^- - D_2$ anion complex

D. A. Wild[a] and E. J. Bieske[b]
School of Chemistry, The University of Melbourne, Melbourne 3010, Australia

(Received 17 September 2004; accepted 30 September 2004)

The infrared spectrum of the $I^- - D_2$ anion complex is measured in the D_2 stretch region by monitoring production of I^- photofragments. The rotationally resolved spectrum consists of two overlapping Σ-Σ subbands, redshifted by ≈ 58 cm^{-1} from the free D_2 fundamental vibrational band. These subbands are associated with absorptions by $I^- - D_2$ complexes containing *ortho* and *para* forms of D_2. The measured rotational constants are consistent with a 3.79 Å separation between I^- and the D_2 center of mass, contracting by 0.08 Å when the D_2 subunit is vibrationally excited. Spectroscopic data are used to generate effective radial potential energy curves describing the interaction of *ortho* and *para* D_2 with I^- from which the dissociation energies of $I^- - D_2$(*ortho*) and $I^- - D_2$(*para*) are estimated as $D_0 = 236$ and 297 cm^{-1}, respectively. © *2004 American Institute of Physics.* [DOI: 10.1063/1.1822920]

I. INTRODUCTION

High-resolution spectra of weakly bound complexes and clusters provide valuable data for developing and assessing intermolecular potential energy surfaces.[1–3] Although the majority of spectroscopic investigations have focussed on neutral van der Waals complexes, in recent years high-resolution spectra have also been obtained for charged species.[4] Anion complexes have proved particularly challenging targets and currently the only fully rotationally resolved IR spectra are for the halide-H_2 dimers ($Cl^- - H_2$, $Cl^- - D_2$, $Cl^- - HD$, $Br^- - H_2$, $Br^- - D_2$, and $I^- - H_2$; Refs. 5–9). The present study of $I^- - D_2$ continues and complements this earlier work.

Spectroscopic and theoretical studies have shown that the H_2 molecule tends to establish a linear hydrogen bond with halide anions.[5–8,10] While the integrity of the H_2 subunit is largely maintained in the complex, formation of the H bond is accompanied by marginal proton transfer towards the halide, which is manifested in a redshift of the H–H stretching frequency. The extent of the proton transfer, magnitude of the redshift, and dissociation energy of the complexes all track the proton affinity of the halide anion, decreasing in the order $F^- > Cl^- > Br^- > I^-$.

Due to the low masses and large rotational constants of the H_2 and D_2 molecules, the halide-H_2 and halide-D_2 complexes are floppy and zero-point excursions are substantial. Tunnelling between equivalent linear minima through a *T*-shaped transition state plays a particularly significant role. Experimentally, the consequences of this tunnelling have been observed in the D–D stretch bands of $Cl^- - D_2$ and $Br^- - D_2$ through a doubling of each rovibrational line (separation ≈ 0.24 cm^{-1} for $Cl^- - D_2$ and 0.57 cm^{-1} for $Br^- - D_2$). The lines' separation is related to the *difference* in the tunnelling splittings for $X^- - D_2$ complexes governed by the effective $X^- + D_2(v_{DD}=0)$ and $X^- + D_2(v_{DD}=1)$ potential energy surfaces. Due to the larger ionic radius of I^-, one might anticipate that the intermolecular bond in $I^- - D_2$ is longer and weaker than it is in $Cl^- - D_2$ and $Br^- - D_2$ and that the tunnelling splittings will be larger.

The spectroscopic data for $I^- - D_2$ presented in this paper together with information previously gathered for $I^- - H_2$ should in the future prove useful for testing *ab initio* potential energy surfaces describing the $I^- + H_2$ interaction and, more generally, for assessing the efficacy of different *ab initio* approaches for dealing with heavier anions.

II. EXPERIMENTAL METHODS

Details of the experimental arrangement can be found in Refs. 5 and 11. Briefly, the infrared spectrum of $I^- - D_2$ was obtained by monitoring production of I^- photofragments as the IR wavelength was scanned over the D–D stretch region. The experimental setup is essentially a home-built tandem mass spectrometer equipped with an ion source designed to generate cooled cluster ions. The mass spectrometer consists of a primary quadrupole mass filter for selection of $I^- - D_2$ ions, an octopole ion guide where the ions are overlapped with the counterpropagating output of a pulsed tuneable IR OPO (Continuum Mirage 3000 OPO, ≈ 0.017 cm^{-1} bandwidth), and a second quadrupole mass filter tuned to the mass of the daughter I^- ions. The I^- photofragments were sensed with a channel plate detector. Wavelength calibration was accomplished using a wave meter (New Focus 7711) to measure the wavelength of the signal output from the first stage of the optical parametric oscillator, and the 532 nm output of the seeded Nd YAG laser. Line wave numbers were corrected by $+0.04$ cm^{-1} to account for the Doppler shift arising from the ions' 10 eV kinetic energy in the octopole ion guide where they interacted with the IR beam.

The $I^- - D_2$ complexes were produced in an electron beam crossed supersonic expansion of Ar seeded with 5% D_2 and traces of CH_3I as a source of I^-. Optimum complex formation required relatively small separation between the

[a]Present address: M.P.I. für biophysikalische Chemie, 37077 Göttingen, Germany.
[b]Electronic mail: evanjb@unimelb.edu.au

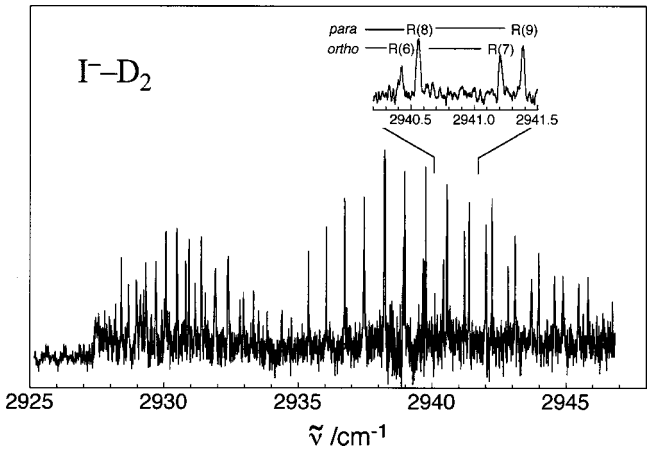

FIG. 1. Infrared spectrum of I^-D_2. The spectrum contains two Σ-Σ subbands associated with complexes containing *ortho* and *para* D_2 molecules (see inset).

nozzle orifice and the electron impact zone, suggesting that D_2 molecules attach to iodide ions through three-body association reactions in the initial part of the expansion. Owing to limited D_2 availability it was not possible to fully optimize I^-D_2 production. Consequently, the signal-to-noise ratio of the spectrum is inferior to that of the previously reported I^-H_2 spectrum.[7]

III. RESULTS AND ANALYSIS

The infrared spectrum of I^-D_2 in the D–D stretch region (2925–2947 cm^{-1} range) is displayed in Fig. 1. The D–D stretch band is redshifted by $\approx$58 cm^{-1} from the transition of the free D_2 molecule. The relative shift of the band ($\Delta\nu/\nu_{DD}=0.019$) is very similar to that of I^-H_2 ($\Delta\nu/\nu_{RH}=0.018$). The spectrum comprises two overlapping Σ-Σ subbands that are associated with complexes containing *para* and *ortho* D_2 (see inset to Fig. 1). Altogether 25 lines were assigned to $I^-D_2(o)$ and 27 lines to $I^-D_2(p)$. Line wave numbers for the two bands were separately fitted using a linear pseudodiatomic transition energy expression,

$$\nu_{obs}=\nu_o+B'[J'(J'+1)]-D'[J'(J'+1)]^2 - B''[J''(J''+1)]+D''[J''(J''+1)]^2. \quad (1)$$

The fitted spectroscopic constants are listed in Table I. The origin of the $I^-D_2(o)$ band lies 1.45 cm^{-1} to higher energy from that of $I^-D_2(p)$, but aside from this the spectroscopic constants for the two forms are the same within experimental error.

One can conclude that I^-D_2 essentially consists of an I^- anion weakly attached to a D_2 molecule firstly because the D–D vibrational transition of I^-D_2 is only slightly shifted from that D_2, and second because the only observed photofragment is I^-. Vibrationally averaged intermolecular separations, harmonic intermolecular stretching frequencies, and force constants are listed in Table I. The effective intermolecular separations between the I^- and the D_2 center of mass were estimated using

TABLE I. Constants for I^-D_2 obtained by fitting rovibrational line positions. The 2σ errors in the last significant figure(s) are given in brackets. The R''_{cm} and R'_{cm} values are ground and excited state vibrationally averaged equilibrium separations estimated from Eq. (2). The $I^-D_2(o)$ and $I^-D_2(p)$ band shifts are given relative to the $Q_1(0)$ and $Q_1(1)$ transitions of D_2 (2993.57 and 2991.46 cm^{-1} from the constants in Ref. 12). Harmonic intermolecular stretching frequencies ω_s and force constants k_s are estimated from Eq. (3). The I^-H_2 data are from Ref. 7.

	$I^-D_2(o)$	$I^-D_2(p)$	$I^-H_2(o)$
ν_0 (cm^{-1})	2935.60(8)	2934.16(8)	4081.11(8)
$\Delta\nu_0$ (cm^{-1})	−58.0	−57.3	−74.1
B'' (cm^{-1})	0.2979(10)	0.2983(10)	0.5683(14)
D''($\times10^{-5}$ cm^{-1})	1.6(4)	1.3(4)	6.7(4)
B' (cm^{-1})	0.3105(10)	0.3107(10)	0.6023(12)
D'($\times10^{-5}$ cm^{-1})	1.6(4)	1.4(4)	6.0(4)
R''_{cm} (Å)	3.790(6)	3.788(6)	3.851(5)
R'_{cm} (Å)	3.711(6)	3.710(6)	3.739(4)
k''_s (N/m)	1.5(4)	1.8(6)	1.27(9)
k'_s (N/m)	1.7(4)	1.9(6)	1.68(13)
ω''_s (cm^{-1})	81(10)	90(14)	104(4)
ω'_s (cm^{-1})	86(11)	92(13)	120(5)

$$R_{cm}=\sqrt{\frac{F}{\mu_{com}}\left(\frac{1}{B_{com}}-\frac{\langle 1+\mathrm{Cos}^2\,\theta\rangle}{2b_{DD}}\right)}, \quad (2)$$

where $F=16.857\,63$ amu cm^{-1} Å^2, b_{DD} is the D_2 rotational constant ($b''_{DD}=29.91\,cm^{-1}$, $b'_{DD}=28.85\,cm^{-1}$, Ref. 12), B_{com} is the rotational constant of the complex, μ_{com} is the reduced mass of the complex (in amu), and θ is the angle between the diatomic and intermolecular bonds. Estimates for $\langle 1+\mathrm{Cos}^2\,\theta\rangle$ near R_{cm} were obtained using the hindered rotor model described in Sec. IV and are listed in Table II. Harmonic intermolecular stretching frequencies were estimated from the rotational constants using the expression[13]

$$\omega_s=\sqrt{\frac{4B_{com}^3}{D_{com}}\left(1-\frac{B_{com}}{b_{DD}}\right)}. \quad (3)$$

IV. EMPIRICAL INTERMOLECULAR RADIAL POTENTIALS

The rotational and centrifugal distortion constants were used as ingredients to develop four radial intermolecular potential energy curves describing the interactions of I^- with $D_2(ortho,v_{DD}=0)$, $D_2(para,v_{DD}=0)$, $D_2(ortho,v_{DD}=1)$,

TABLE II. Parameters for BO-RKR radial potential curves of $I^-D_2(o)$ and $I^-D_2(p)$ [Eqs. (4)–(7)]. For all four potential curves, the short-range Morse potential is joined to the long-range BO potential at $R_j=4.25$ Å using the switching functions given in Eq. (7), with $w=10$ $Å^{-1}$.

	$I^-D_2(o)$		$I^-D_2(p)$	
	$v_{DD}=0$	$v_{DD}=1$	$v_{DD}=0$	$v_{DD}=1$
$\langle\mathrm{Cos}^2\,\theta\rangle$	0.76	0.76	0.76	0.77
D_e (cm^{-1})	280	325	345	389
β	4.87	4.66	4.82	4.50
R_e (Å)	3.719	3.647	3.724	3.652
a_0 (cm^{-1})	0	0	59.8	57.7
a_3($\times10^3$ cm^{-1} Å^3)	1.327	0.261	7.635	8.124
a_4($\times10^4$ cm^{-1} Å^4)	1.360	2.584	2.762	3.004
a_5($\times10^5$ cm^{-1} Å^5)	2.088	2.064	1.070	1.187

and $D_2(para, v_{DD}=1)$. The procedure for generating the potentials is fully described in earlier publications.[6,8] Briefly, the rotational and centrifugal distortion constants are used as inputs for a rotational RKR procedure[14,15] to define a Morse potential appropriate for the effective radial potential near the minimum,

$$V_M(R) = a_o + D_e(e^{-2\beta(x-1)} - 2e^{-\beta(x-1)}), \tag{4}$$

where $x = R/R_e$.

At longer ranges the effective radial potential is defined by solving the hindered rotor Hamiltonian at a series of fixed intermolecular separations. This assumes that the radial vibrational motion is governed by an effective potential defined by averaging over the faster bending/hindered rotation motion in what amounts to a Born-Oppenheimer (BO) separation. The angular dependence of the intermolecular interaction is obtained by considering the charge-quadrupole and induction interactions between the halide and the D_2 molecule. Vibrationally averaged quadrupole moments and polarizabilities for D_2 are taken from Ref. 16. At each separation the lowest energy solution is allied with a wave function that is symmetric with respect to exchange of the two D atoms and is associated with I^- interacting with *ortho* D_2. The antisymmetric state lies higher in energy and is associated with I^- interacting with *para* D_2. The lowest eigenvalues of the hindered rotor Hamiltonian are subsequently fitted to an inverse power series in R,

$$V_{lr}^{BO}(R) = a_0 - \frac{a_3}{R^3} - \frac{a_4}{R^4} - \frac{a_5}{R^5}, \tag{5}$$

where a_0 corresponds to the energy of the dissociation limit. For $I^- - D_2(ortho)$ the dissociation limit corresponds to $I^- + D_2(j=0)$ so that $a_0 = 0$, whereas for $I^- - D_2(para)$ the dissociation limit corresponds to $I^- + D_2(j=1)$ so that $a_0 = 2b_{DD}$. The Morse and long-range potentials [$V_M(R)$ and $V_{lr}^{BO}(R)$] are spliced to give the total potential,

$$V_{tot}(R) = f(R)V_M(R) + g(R)V_{lr}^{BO}(R), \tag{6}$$

where $f(R)$ and $g(R)$ are switching functions

$$f(R) = 0.5\{\tanh[w(R_j - R)] + 1\}$$
$$g(R) = 0.5\{\tanh[w(R - R_j)] + 1\}. \tag{7}$$

For all four potential energy curves, the short-range Morse potential is joined to the long-range BO potential at $R_j = 4.25$ Å using the switching functions with $w = 10\ \text{Å}^{-1}$. Parameters for the potential energy curves are provided in Table II.

The BO-RKR curves for $I^- + D_2(o)(v_{DD}=0)$ and $I^- + D_2(p)(v_{DD}=0)$ are plotted together in Fig. 2. Near the equilibrium separation ($R_e = 3.72$ Å) the two curves are very similar, but at longer range the $I^- + D_2(p)(v_{DD}=0)$ curve, which has as its asymptote the $I^- + D_2(v_{DD}=0, j=1)$ limit, is more attractive. The $I^- + D_2(o)(v_{DD}=0)$ curve is predicted to have a depth of 280 cm^{-1} ($D_0 = 236\ cm^{-1}$) whereas the depth of the $I^- + D_2(p)(v_{DD}=0)$ curve is 345 cm^{-1} ($D_0 = 297\ cm^{-1}$). It is worth noting that there is a minor inconsistency in the empirical curves. The wave function for the lowest energy level of the complex is symmetric with respect to exchange of the D atoms and should be associated with the $I^- + D_2(o)(v_{DD}=0)$ curve. However, the empirical $I^- + D_2(p)(v_{DD}=0)$ curve is slightly deeper than the $I^- + D_2(o)(v_{DD}=0)$ curve so that the ground intermolecular stretch level of the former is predicted to lie slightly lower than the latter (by $\approx 1\ cm^{-1}$). This inconsistency probably relates to the relatively large errors ($\approx 20\%$) in the measured centrifugal distortion constants that are used in the generation of the empirical potential curves.

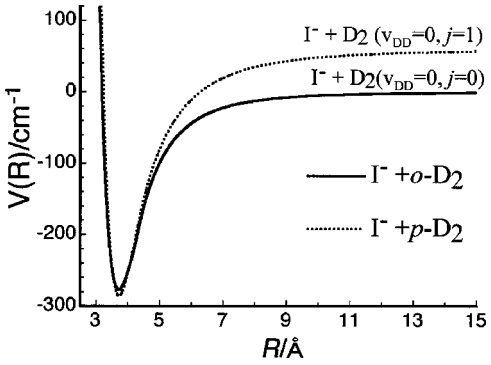

FIG. 2. Effective radial potential energy curves for I^- interacting with *ortho* D_2 and *para* D_2. Parameters and properties of the curves are given in Tables II and III.

As a second example the $I^- + D_2(o)(v_{DD}=0)$ and $I^- + D_2(o)(v_{DD}=1)$ potential curves are plotted in Fig. 3. The effects of vibrationally exciting the D_2 subunit are clearly apparent; the $v_{DD}=1$ curve is $\approx 45\ cm^{-1}$ deeper than the $v_{DD}=0$ curve and the equilibrium separation is reduced by 0.072 Å. The vibrationally mediated enhancement of the $I^- + D_2$ intermolecular interaction is due to increases in the vibrationally averaged polarizability and quadrupole moment

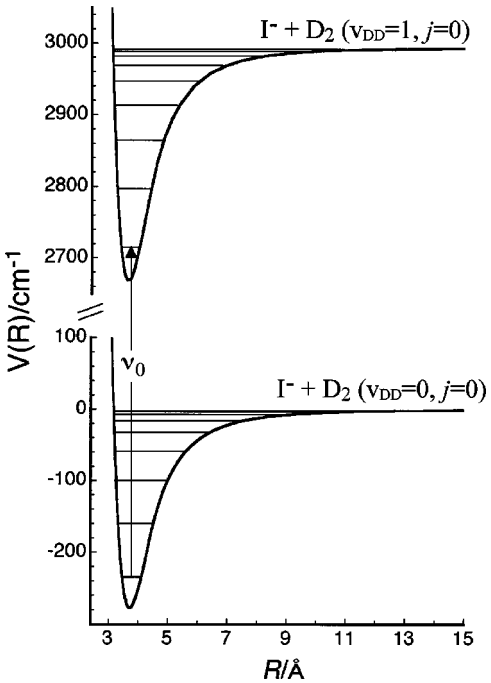

FIG. 3. Effective radial potential energy curves for I^- interacting with *ortho* D_2 in the $v_{DD}=0$ and $v_{DD}=1$ vibrational states. Parameters and properties of the curves are given in Tables II and III.

TABLE III. Potential well depths D_e, dissociation energies D_0, and vibrational energy level spacings for the BO-RKR potential curves of I^-–$D_2(o)$ and I^-–$D_2(p)$. The vibrational band shift $\Delta\nu$ is the difference in D_0 values for the $v_{DD}=0$ and $v_{DD}=1$ curves. All values are in cm^{-1}. The number of bound stretching levels supported by each potential curve is also given.

	I^-–$D_2(o)$		I^-–$D_2(p)$	
	$v_{DD}=0$	$v_{DD}=1$	$v_{DD}=0$	$v_{DD}=1$
D_e	280	325	345	389
D_0	236	279	297	340
$\Delta\nu_{DD}$	−43		−43	
$E(1,0)$	77	82	85	88
$E(2,0)$	138	150	151	160
$E(3,0)$	179	199	198	215
$E(4,0)$	206	233	232	255
$E(5,0)$	222	255	256	284
	9 levels	10 levels	10 levels	12 levels

of the D_2 upon going from $v_{DD}=0$ to $v_{DD}=1$. The difference in D_0 values for the two curves in Fig. 3 should correspond to the red shift of the D–D stretch transition of I^-–D_2 with respect to the D–D stretch transition of the free D_2 molecule. In fact, $D_0-D_o'=-43\,cm^{-1}$ around 20% less than the experimentally observed redshift ($\approx -58\ cm^{-1}$).

At this stage there are no other experimental or theoretical data against which to test the I^-–D_2 BO-RKR curves. However, it should be remarked that similar curves developed for Cl^-–H_2 and Cl^-–D_2 yield predictions for dissociation energies that accord well with recent *ab initio* and rovibrational calculations.[17,18]

V. DISCUSSION

A. General

The spectroscopic data and BO-RKR potential curves provide a view of the way in which an I^- ion interacts with a D_2 molecule. Predictably the properties of the I^-–D_2 complex are very similar to those of the previously characterized I^-–H_2 complex, and more generally with those of the Cl^-–H_2, Cl^-–D_2, Br^-–H_2, and Br^-–D_2 systems. In each case the H–H (D–D) stretch band possesses a Σ-Σ structure demonstrating that the complexes possess linear equilibrium geometries as expected from consideration of the long-range electrostatic interaction between the halide anion and the quadrupole moment on the H_2 or D_2 molecule (attractive for a linear geometry and repulsive for a *T*-shaped configuration). Vibrationally averaged intermolecular separations, deduced from the rotational constants assuming an undistorted D_2 monomer, are 3.789 ± 0.006 Å for I^-–$D_2(o)$ and 3.786 ± 0.006 Å for I^-–$D_2(p)$. The vibrationally averaged intermolecular bond distances for I^-–$D_2(o)$ and I^-–$D_2(p)$ are slightly less (by 0.06 Å) than that previously determined for I^-–$H_2(o)$ (3.851 Å),[7] the difference being due to greater zero point motion in the intermolecular stretch and bend coordinates for the I^-–H_2 system. Exciting the D_2 subunit to $v_{DD}=1$ results in a shortening and stiffening of the intermolecular bond ($\Delta R_{cm}=-0.079$ Å). These effects, which are discernible in the $I^-+D_2\,(v_{DD}=0)$ and $I^-+D_2\,(v_{DD}=1)$ potential energy curves in Fig. 3, are attributable to increases in the quadrupole moment and polarizabilities of D_2 in the $v_{DD}=1$ state.

Large amplitude tunnelling motion between equivalent linear configurations of I^-–D_2, corresponding to exchange of the two D atoms, is manifested as a tunnelling splitting of the energy levels. The wave function associated with the lower tunnelling level is symmetric with respect to the tunnelling coordinate and correlates with I^- interacting with *ortho* D_2 (even D_2 rotational levels), while the upper level is antisymmetric and correlates with I^- interacting with *para* D_2 (odd D_2 rotational levels).[19] Interconversion between symmetric (*ortho*) and antisymmetric (*para*) forms through radiative or collisional processes is expected to be extremely inefficient, making it convenient to consider I^-–$D_2(o)$ and I^-–$D_2(p)$ as distinct species. In the limit of an infinite barrier for internal rotation, the energy levels (and IR spectra) of I^-–$D_2(p)$ and I^-–$D_2(o)$ would coincide, while at the other extreme, for entirely unhindered internal rotation, the *ortho/para* levels would be separated by $\approx 2b_{DD}=59.8\,cm^{-1}$. In fact, the tunnelling barrier for I^-–D_2 lies between these two extremes and depends upon the vibrational state of the D_2 subunit. As the quadrupole moment of D_2 increases by ≈8% when it is excited from the $v_{DD}=0$ to the $v_{DD}=1$ vibrational state,[16] the effective tunnelling barrier should be larger in the upper state, reducing the *ortho/para* splitting. For this reason, the I^-–$D_2(p)$ transitions occur at lower energy (by 1.45 cm^{-1}) than the corresponding transitions of I^-–$D_2(o)$ (Fig. 1).

The relative stabilities of I^-–$D_2(o)$ and I^-–$D_2(p)$ play a key role in deciding their populations in the ion source, and therefore the relative intensities of the two subbands in Fig. 1. Initially it may seem surprising that the I^-–$D_2(o)$ lines are weaker than the I^-–$D_2(p)$ lines (the intensity ratio is ≈0.6), given that the *ortho/para* population ratio is 2:1 for natural D_2 gas. The cause, as explained in Refs. 6 and 8 in relation to Cl^-–D_2 and Br^-–D_2, is that I^-–$D_2(p)$ is $\approx 2b_{DD}$ more stable than I^-–$D_2(o)$ ($D_0=297$ vs $235\ cm^{-1}$) and thus favored in the low temperature supersonic expansion of the ion source. Any I^-–$D_2(o)$ complexes that are formed are liable to be converted to I^-–$D_2(p)$ in the early part of the expansion through the exothermic I^-–$D_2(o)+D_2(p)\rightarrow I^-$–$D_2(p)+D_2(o)$ ligand switching reaction.

The rotational temperatures of the I^-–$D_2(o)$ and I^-–$D_2(p)$ populations, estimated from intensities of the less congested *R*-branch lines, are both ≈40 K, similar to the temperature of Br^-–$D_2(o)$ and Br^-–$D_2(p)$ complexes investigated previously.[8] If one assumes that the I^-–$D_2(o)+D_2(p)\rightarrow I^-$–$D_2(p)+D_2(o)$ ligand exchange reaction is exothermic by $2b_{DD}\approx 60\,cm^{-1}$ and had reached equilibrium at the complexes' effective rotational temperature, the ratio of the I^-–$D_2(o)$ to I^-–$D_2(p)$ populations would be roughly 0.25. This is somewhat lower than the observed population ratio of 0.6 deduced from the relative intensities of the rovibrational lines. The discrepancy perhaps indicates that the ligand exchange process in fact does not reach equilibrium in the expansion, and terminates earlier than the rotational cooling. It is worth commenting that the corresponding X^-–$H_2(p)+H_2(o)\rightarrow X^-$–$H_2(o)\rightarrow H_2(p)$ (X=Cl,Br,J)

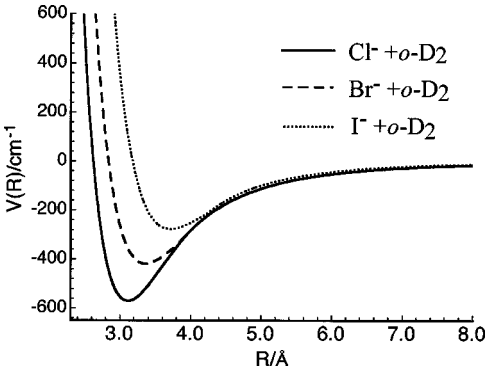

FIG. 4. Effective radial potential energy curves for $Cl^- + D_2(o)$, $Br^- + D_2(o)$, and $I^- + D_2(o)$.

ligand exchange processes, which are exothermic by $2b_{HH} \approx 120\,cm^{-1}$, are so efficient that only the $X^- - H_2(o)$ species have been observed.[6,7]

B. Comparison of $Cl^- - D_2$, $Br^- - D_2$, and $I^- - D_2$

The current study enables us to compare the properties of $I^- - D_2$ with those of $Cl^- - D_2$ and $Br^- - D_2$ whose rotationally resolved infrared spectra were reported previously.[6,8] Differences between interactions in the three systems are exemplified in Fig. 4 where effective radial BO-RKR curves for $I^- + D_2(o)$, $Br^- + D_2(o)$, and $Cl^- + D_2(o)$ are plotted together. The long-range parts of the curves, which are generated by considering the induction and electrostatic interactions are almost identical. Predictably, as the halide becomes larger, the well depth diminishes and the radial equilibrium separation increases ($R_e = 3.11$ Å and $D_0 = 499\,cm^{-1}$ for $Cl^- - D_2$, $R_e = 3.36$ Å and $D_0 = 364\,cm^{-1}$ for $Br^- - D_2$, and $R_e = 3.72$ Å and $D_0 = 235\,cm^{-1}$ for $I^- - D_2$). The comparatively weak intermolecular interaction for $I^- - D_2$ is reflected in the magnitude of the D_2 vibrational band shift ($\approx 58\,cm^{-1}$), which is smaller than those of $Br^- - D_2$ and $Cl^- - D_2$ (85 and 114 cm^{-1}, respectively). Perhaps surprisingly, the intermolecular bond contractions following vibrational excitation of the D_2 subunit are similar for $I^- - D_2$, $Br^- - D_2$, and $Cl^- - D_2$ ($\Delta R_{cm} = -0.079$, -0.076, and -0.078 Å, respectively).

C. Vibrational predissociation

Widths of the $I^- - D_2$ rovibrational lines are close to the bandwidth of the OPO output ($\approx 0.017\,cm^{-1}$). Any contribution to the lines' widths from homogeneous lifetime broadening is estimated to be less than $0.01\,cm^{-1}$, implying that vibrational predissociation proceeds on a time scale exceeding 530 ps. An upper limit for the time scale of the fragmentation process is provided by the observation that dissociation ensues during the ions' passage through the octopole region of the apparatus ($\approx 50\,\mu s$). As far as we could ascertain, there was neither a J dependence for the line widths nor any difference between the predissociation rates of $I^- - D_2(o)$ and $I^- - D_2(p)$. The observations are consistent with trends deduced from earlier studies of $F^- - H_2$, $Cl^- - H_2$, $Cl^- - D_2$, $Br^- - H_2$, $Br^- - D_2$, and $I^- - H_2$. Generally, the vibrational predissociation rate diminishes as the halide becomes larger, and is also reduced when H_2 is replaced by D_2.

VI. CONCLUSIONS

Outcomes of the current work can be summarized as follows.

(1) The D–D stretch band of $I^- - D_2$ is redshifted by $\approx 58\,cm^{-1}$ from the free D_2 molecule absorption and is composed of two Σ-Σ subbands, separated by $1.45\,cm^{-1}$, corresponding to absorptions by $I^- - D_2(ortho)$ and $I^- - D_2(para)$.

(2) The $I^- - D_2$ complex possesses a linear equilibrium structure with a vibrationally averaged intermolecular separation of 3.79 Å.

(3) Vibrational excitation of the D_2 subunit leads to a 0.079 Å contraction of the $I^- - D_2$ intermolecular bond.

(4) Effective dissociation energies of 235 and 297 cm^{-1} are deduced for $I^- - D_2(ortho)$ and $I^- - D_2(para)$, respectively.

(5) Linewidths are limited by the light source bandwidth ($0.017\,cm^{-1}$), demonstrating that predissociation takes place on a time scale exceeding 530 ps following vibrational excitation of the D_2 subunit.

Developing accurate *ab initio* surfaces describing negatively charged complexes containing the heavier halides remains a challenging enterprise. Reproduction of the rotational constants and vibrational frequencies for $I^- - D_2$ reported in this paper along with previously reported spectroscopic data for $I^- - H_2$ should serve as critical tests for three-dimensional *ab initio* potential energy surfaces describing the $I^- + H_2$ interaction.

ACKNOWLEDGMENTS

The authors gratefully acknowledge support from the Australian Research Council and the University of Melbourne.

[1] J. M. Hutson, Annu. Rev. Phys. Chem. **41**, 123 (1990).
[2] A. van der Avoird, P. E. S. Wormer, and R. Moszynski, Chem. Rev. (Washington, D.C.) **94**, 1931 (1994).
[3] Z. Bacic and R. E. Miller, J. Phys. Chem. **100**, 12945 (1996).
[4] E. J. Bieske and O. Dopfer, Chem. Rev. (Washington, D.C.) **100**, 3963 (2000).
[5] D. A. Wild, R. L. Wilson, P. S. Weiser, and E. J. Bieske, J. Chem. Phys. **113**, 10154 (2000).
[6] D. A. Wild, P. S. Weiser, E. J. Bieske, and A. Zehnacker, J. Chem. Phys. **115**, 824 (2001).
[7] D. A. Wild, Z. M. Loh, R. L. Wilson, and E. J. Bieske, J. Chem. Phys. **117**, 3256 (2002).
[8] D. A. Wild, P. S. Weiser, and E. J. Bieske, J. Chem. Phys. **115**, 6394 (2001).
[9] R. L. Wilson, Z. M. Loh, D. A. Wild, E. J. Bieske, and A. Buchachenko, J. Chem. Phys. **121**, 2085 (2004).
[10] D. A. Wild, R. L. Wilson, Z. M. Loh, and E. J. Bieske, Chem. Phys. Lett. **393**, 517 (2004).
[11] P. S. Weiser, D. A. Wild, and E. J. Bieske, Chem. Phys. Lett. **299**, 303 (1999).

[12] K. P. Huber and G. Herzberg, *Molecular Spectra and Molecular Structure IV. Constants of Diatomic Molecules* (van Nostrand Reinhold, New York, 1979).
[13] D. J. Millen, Can. J. Chem. **63**, 1477 (1985).
[14] M. S. Child and D. J. Nesbitt, Chem. Phys. Lett. **149**, 404 (1988).
[15] D. J. Nesbitt, M. S. Child, and D. C. Clary, J. Chem. Phys. **90**, 4855 (1989).
[16] J. L. Hunt, J. D. Poll, and L. Wolniewicz, Can. J. Phys. **62**, 1719 (1984).
[17] M. H. Alexander, J. Chem. Phys. **118**, 9637 (2003).
[18] A. A. Buchachenko, T. A. Grinev, J. Klos, E. J. Bieske, M. M. Szczesniak, and G. Chalasinski, J. Chem. Phys. **119**, 12931 (2003).
[19] Even and odd *j* levels of D_2 are associated respectively with the *ortho* and *para* modifications. Note that in Refs. 2 and 3 the *ortho/para* designations for D_2 were mistakenly reversed.